Reference-free quantitative microscopic imaging of coherent arbitrary vectorial light beams

Arthur Baroni, Patrick Ferrand

Research Article | Vol. 28, No. 23 / 9 November 2020 / Optics Express 35339

Optics EXPRESS

Reference-free quantitative microscopic imaging of coherent arbitrary vectorial light beams

ARTHUR BARONI AND PATRICK FERRAND*

Aix-Marseille Univ, CNRS, Centrale Marseille, Institut Fresnel, F-13013 Marseille, France
**patrick.ferrand@fresnel.fr*

Abstract: Precise spatial characterization of vectorial beams is crucial for many advanced optical experiments, but challenging when wavefront and polarization features are involved together. Here we propose a reference-free method aimed at extracting the map of the complex-amplitude components of any coherent beam at an optical-microscopy resolution. Our method exploits recent advances in ptychographic imaging approaches. We emphasize its versatility by reconstructing successfully various experimental vectorial beams including polarization and phase vortices, the exit field of a multicore fiber and a speckle pattern.

1. Introduction

Recently-developed vectorial beams involve complicated spatial distributions of intensity, phase and state of polarization (SoP). When produced intentionally, those beams are expected to provide additional degrees of freedom to light; emblematic examples are vortex beams that are tailored in a twisted fashion in polarization [1] and/or in phase, in order to carry an orbital angular momentum [2]. These specific features are expected to offer progress towards denser information encoding in telecommunications [3], novel conditions of light-matter interaction, optical manipulation [4], materials processing [5], microscopy [6,7] and non-linear optics [2]. These developments were made possible thanks to the emergence of versatile optical light structuration tools such as spatial light modulators [8] or, even more recently, metasurfaces [9]. Scattering by complex media also produces convoluted beams [10]. Measuring such beams allowed quantifying the so-called transmission matrix of the medium, a key parameter for further controlling light propagation in such media [11].

Although nowadays widely present in optical experiments, those valuable vectorial beams remain highly challenging to measure. To a large extent, this results from the mixing of phase and polarization space-variant features, the simultaneous investigations of which being tedious. Since phase is involved, most approaches are interferometric, and adapted to account for polarization [12–14]; however, the precision of the reconstructed field relies on the knowledge of a reference beam. Wavefront-analysis methods have been demonstrated using polarization-sensitive metalens arrays [15], to the price of the limited spatial resolution of the meta-pixel. Another elegant approach uses mode decomposition: the field is interrogated by specific computer-generated phase filters, allowing measuring the complex amplitude of each mode in a complete modal basis [16]. Initially designed for demultiplexing applications and very powerful for this purpose [3], the method could be extended towards vectorial field reconstruction, provided that intermodal and intramodal phases are accurately measured [17] and assuming that the field could be fairly described by a limited number of modes [18]. This method is therefore intrinsically restricted to fields presenting smooth variations, such as vortices created in large-mode-area fibers [17].

Here we propose a method aiming at extracting the spatial map of any arbitrary vectorial complex field. The field distribution is interrogated in an arbitrary plane by a thin moveable object, about which very limited knowledge is required. By analyzing the resulting series of

#408665 https://doi.org/10.1364/OE.408665
Journal © 2020 Received 28 Aug 2020; accepted 5 Oct 2020; published 6 Nov 2020

Optics EXPRESS

diffraction patterns and by exploiting recent advances in phase-retrieval imaging methods, namely vectorial ptychography, complete field maps are reconstructed. Fields distributions such as vortex beams, multicore fiber exit field and vectorial speckles are experimentally investigated and reconstructed, confirming the resolution and the versatility of the method.

2. Theory

A coherent vectorial beam $\mathbf{E}(\mathbf{r})$, in the paraxial approximation, can be described by the complex amplitude spatial distribution of each of its two components, i. e.,

$$\mathbf{E}(\mathbf{r}) = \begin{bmatrix} E_x(\mathbf{r}) \\ E_y(\mathbf{r}) \end{bmatrix}, \tag{1}$$

where x and y refer to a cartesian coordinate system in the propagation transverse plane. At any position $\mathbf{r}$ in this plane, the vector $\mathbf{E}(\mathbf{r})$ is proportional to a normalized Jones vector [19], whose phase relationship between the two components $E_x(\mathbf{r})$ and $E_y(\mathbf{r})$ informs about the local SoP. On the other hand, the *spatial* variations of the phases of E_x and E_y are associated to the two wavefronts, i. e., one for each component.

Since phase and polarization measurements are required, we propose in this work to exploit recent progress in phase-retrieval imaging by means of vectorial ptychography [20]. Vectorial ptychography involves (i) an investigated object $\mathbf{J}$ that is illuminated at successive overlapping positions by a finite-size spatially-coherent vectorial beam $\mathbf{E}$ (Eq. (1)), and (ii) the recording of the corresponding series of diffraction intensity patterns, after a polarization analyzer. Under the assumption that illumination and object interact in a multiplicative way, the recorded intensity can be written as [20]

$$I_{j,l}(\mathbf{q}) = \left| \mathcal{F}\left[\mathbf{A}_l \times \mathbf{J}(\mathbf{r} - \mathbf{r}_j) \times \mathbf{E}(\mathbf{r}) \right] \right|^2, \tag{2}$$

where $\mathbf{q}$ refers to the reciprocal-space coordinates of the diffraction pattern, $\mathcal{F}$ to a vectorial field propagator, $\mathbf{r}_j$ to the j-th scan position, $\mathbf{A}_l$ is the Jones matrix of the polarization analyzer,

$$\mathbf{J}(\mathbf{r}) = \begin{bmatrix} J_{xx}(\mathbf{r}) & J_{yx}(\mathbf{r}) \\ J_{xy}(\mathbf{r}) & J_{yy}(\mathbf{r}) \end{bmatrix} \tag{3}$$

is the Jones matrix map of the object, and '$\times$' refers here to the matrix multiplication.

In most previous versions of ptychography, both object and illumination were modeled as *scalar* quantities [21]. Their reconstructions could be performed simultaneously by phase retrieval algorithms, thanks to the diversity introduced by the ptychographic scan [22,23]. Here in comparison, the *vectorial* formalism of Eq. (2) is a generalization that brings a significant increase of complexity to the problem, due to the introduction of new degrees of freedom on both object and illumination. As a consequence, strategies for solving successfully the reconstruction problem require more elaborate measurement schemes [20]. In addition, underdetermination specific to vectorial ptychography require the introduction of some *a priori* knowledge [24].

When an arbitrary object is investigated, previous works have shown that its unambiguous vectorial ptychographic reconstruction was possible using several illuminations, with different sequential SoPs, together with several polarization analyses [20]. The joint reconstruction of the illuminations, in addition to those of the object, was also demonstrated, provided that the SoP of the illumination was known [24].

Here in order to investigate an arbitrary illumination, the *a priori* knowledge must be carried by the object only. Since such assumption relates to the behavior of the object with respect to

Optics EXPRESS

polarization, in a sake of experimental simplicity we propose to consider an optically-isotropic object. Under this assumption, its Jones matrix (Eq. (3)) can be written in the reduced form

$$\mathbf{J}(\mathbf{r}) = T(\mathbf{r}) \begin{bmatrix} 1 & 0 \\ 0 & 1 \end{bmatrix}, \tag{4}$$

where the effective scalar nature of such object appears explicitly. Note that the scalar complex transmittance (amplitude and phase) T can be arbitrary and can vary spatially. Consequently, such object needs to be scanned by only one illumination, in order to be reconstructed unambiguously. Still, the polarization analysis of the transmitted field will be required in order to characterize unambiguously the SoP of the illumination itself.

In a nutshell, the exhaustive investigation of an arbitrary vector beam consists in interrogating it by scanning an isotropic object in the desired plane, and by recording series of diffraction intensity patterns for three analysis directions, as illustrated in Fig. 1. Then the field $\mathbf{E}$ can be numerically reconstructed together with the object $\mathbf{J}$ by regular vectorial ptychography with the same criteria and iterative algorithm as detailed in [24]. As classically in ptychography, the success of the reconstructions relies (i) on the good spatial diversity of the object, meaning containing enough spatial features to significantly diffract light [23], and (ii) on the limited size of the illumination beam [21]. Here because the object reconstruction is not the purpose, we can limit the object scanning range to the minimal area that is commonly reported, namely twice the size of the beam is each direction, with an overlap between scanning positions between 60% and 85% of the beam diameter [26]. This leads to a minimal scan of 7×7 points, with a step size of 16% of the beam diameter.

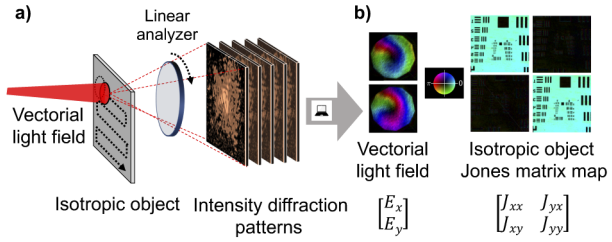

Fig. 1. Vectorial ptychography in the context of arbitrary vectorial beam reconstruction. (a) Principle of the measurement. The vectorial beam is interrogated by a optically-isotropic scanned object. Series of intensity patterns are recorded, after polarization analysis. See Ref. [25] for a detailed optical bench. (b) Example of reconstructed results, after data processing.

3. Experiments

In the sake of generality, the method has been demonstrated experimentally on various convoluted vectorial fields, including (i) a linearly azimuthally polarized vortex beam, (ii) a circularly polarized phase vortex beam, (iii) the exit field of a multicore fiber, and (iv) a vectorial speckle field. In order to emphasize the flexibility of the method and its capability to deal with uneven field distributions, each beam was generated with a significantly asymmetry in phase, amplitude and polarization.

3.1. Optical bench

All acquisitions were carried out on a custom setup detailed in [25]. The scanned object was a 1951 USAF resolution target (R3L1S4P, Thorlabs), meeting both criteria of optical isotropy and spatial diversity. The investigated beams were produced at a wavelength $\lambda = 635$ nm by a weakly

Optics EXPRESS

collimated polarized laser source (S1FC635MP, Thorlabs). The condition of finite support that is required for the reconstruction was fulfilled by restricting spatially the beam to a diameter of about 500 μm, by means of an iris diaphragm placed in the image plane of a microscope, in a so-called selected-area configuration [25]. The 14-bit 1280×960 camera sensor was placed at a distance $d = 190$ mm after the diaphragm, in order to measure the radiated near field [24]. The effective camera pixel size was 25.8×25.8 μm^2 after numerical 4×4 binning, resulting in an effective binned pixel depth of 18 bits.

3.2. Measurements

The linearly azimuthally polarized vortex was produced by illuminating a S-waveplate (RPC-632-02, Altechna) with the laser with a linear SoP oriented at 90° with respect to the S-waveplate alignment mark. The phase vortex beam was created by illuminating the above-mentioned waveplate by a roughly circularly-polarized beam. The fiber exit field was recorded by placing the scanned object at a distance of 30 μm away from end of an aperiodic multicore fiber detailed in [27]. The fiber was significantly bent at 90° in order to induce anisotropy, and illuminated with the laser linearly polarized at 0°, with a slight tilt, in order to create phase variation through the different cores. The speckle field was obtained by illuminating a circular area of diameter 3 mm of a laboratory sealing film (Parafilm, Bemis Company, Inc.) by the above-mentioned azimuthally polarized vortex beam. The scanned object was placed 50 mm after the film. Investigations of the azimuthally polarized vortex, of the phase vortex, and of the speckle field were carried out with a 4× objective lens (ACHN-P, NA 0.1, Olympus). The scanning grid contained 110 points with an average step size of 73 μm along the two raster-scanning directions. All scanning grids include a random fluctuation of maximum amplitude ±50% of the scanning step, in both directions. The reconstructed pixel size was 3.6×4.8 μm^2. The multicore fiber acquisition was performed using a 20× objective lens (ACHN-P, NA 0.45, Olympus), with a scanning grid of 220 points with 10.7 μm average step, leading to a reconstructed pixel size of 0.73×0.97 μm^2. Polarization analysis was performed at angles 0, 60, and 120°.

3.3. Data processing

Each investigated beam was jointly reconstructed together with the scanned object, after 500 iterations of a conjugate gradient algorithm [24]. The object was reconstructed without any isotropy constraint. Then, a small region of interest was arbitrary selected on the retrieved object, and any measured anisotropy was homogeneously removed from the object and transferred onto the illumination, following the method described in [24]. With this procedure, the underdetermination inherent to vectorial ptychography was removed and the global isotropy of the object constitutes a sign of confidence in the reconstructed beam. The reconstructed multicore fiber exit field was numerically back-propagated of (-30) μm before display.

4. Results

4.1. Azimuthally polarized beam

We first present the investigations of the azimuthally polarized beam. The reconstructed Jones map of the object used to interrogate the beam is reported in Fig. 2, showing faithfully reconstructed features. The specimen is isotropic over its whole area, as shown by the map of $\mathbf{J}$, where the agreement with the form of Eq. (4), i. e., $J_{xx} = J_{yy}$ and $J_{yx} = J_{xy} \approx 0$, appears clearly.

The reconstructed beam is shown in Fig. 3. Both complex components maps E_x and E_y are displayed (in Figs. 3(a) and 3(b), respectively) with a color coding emphasizing both amplitude and phase variations, followed by a map of the SoP of the beam (Fig. 3(c)). At first glance the beam appears homogeneous in intensity, with the peculiar decagonal imprint of the iris diaphragm that was used to restrict spatially the imaging field (see section 3.1). Both components

Optics EXPRESS

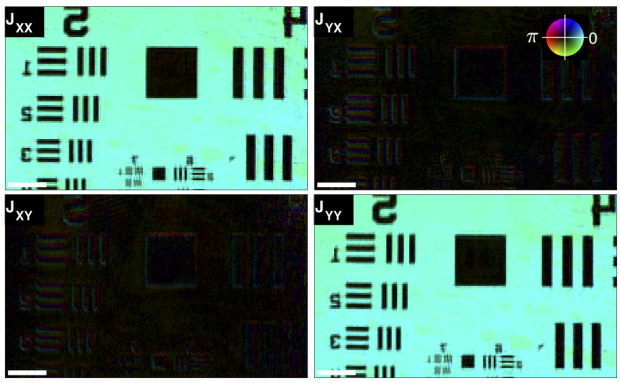

Fig. 2. Reconstructed Jones matrix maps of the scanned object, after data processing of the azimuthally polarized beam. The Inset shows the complex value color coding, with phase encoded as hue and modulus as brightness. Scale bars are 100 μm.

exhibit a slight radial gradient of the phase suggesting a spherical wavefront. The beam shows the expected features of an azimuthally oriented linear-SoP distribution, i. e., dark horizontal and

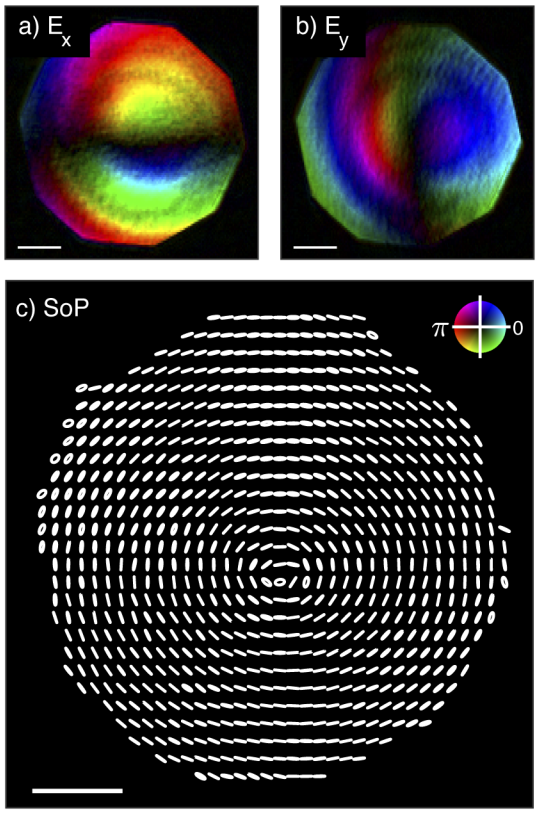

Fig. 3. Reconstructed vectorial field of the azimuthal polarization vortex beam. (a) E_x. (b) E_y. (c) SoP, displayed on a 4×4 pixel grid, for a better readability. Inset shows the complex value color coding, with phase encoded as hue and modulus as brightness. Scale bars are 100 μm.

Optics EXPRESS

vertical strips for E_x and E_y, respectively, giving rise to a central dark singularity in intensity. The phase jumps of π that appear when crossing the dark strips confirm the central symmetry of the field distribution, $E_x(-\mathbf{r}) = -E_x(\mathbf{r})$ and $E_y(-\mathbf{r}) = -E_y(\mathbf{r})$, where $\mathbf{r} = 0$ refers to the beam central singularity. Figure 3(c) confirms that the SoPs are mostly linear, with clear azimuthal orientations, although a weak ellipticity can be noticed in the west-north-west sector.

4.2. Phase vortex beam

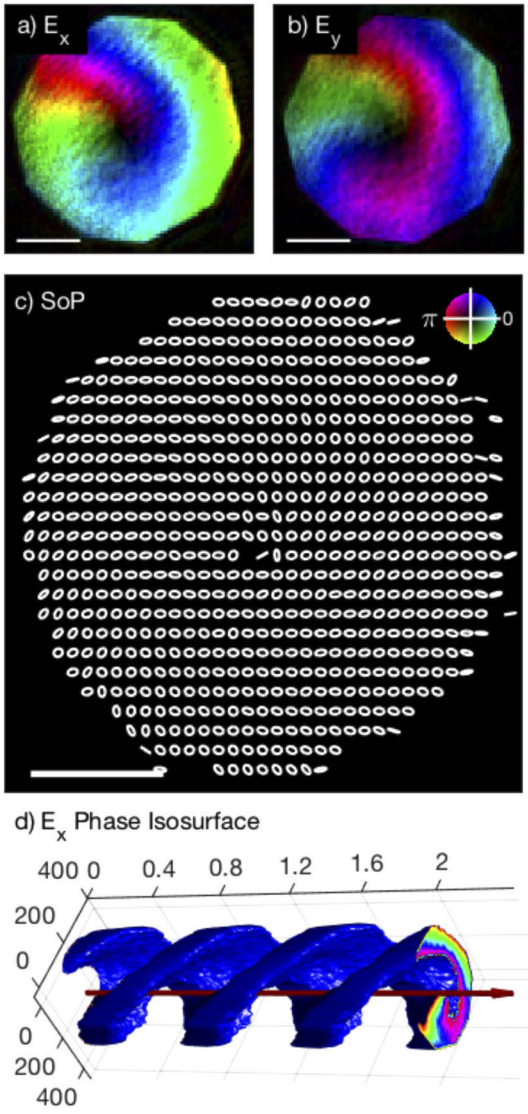

Fig. 4. Reconstructed vectorial field of the phase vortex beam. (a) E_x. (b) E_y. (c) SoP, displayed on a 4×4 pixel grid, for a better readability. Inset shows the complex value color coding, with phase encoded as hue and modulus as brightness. Scale bars are 100 μm. (d) iso-surface plot of the phase of E_x after propagation over 2 μm in the axial direction (red arrow). All dimensions are in μm.

Optics EXPRESS

The results on the phase vortex beam are reported in Fig. 4 (see Supplement 1, Fig. S1 for the reconstructed scanned object). Similarly to the previous case, the field components exhibit a radial phase gradient (Figs. 4(a) and 4(b)), in addition to a central dark spot. Figure 4(c) exhibits highly elliptical SoPs, close to the expected circular ones, over the whole beam section. Here, the beam shows the typical helical phase distribution of an orbital angular momentum, although the superimposed wavefront curvature makes it difficult to quantify its topological charge [2]. This latter is more clearly emphasized by the three-dimensional iso-surface plot of phase of E_x, after numerical propagation along the beam axial direction, and displayed in Fig. 4(d). The axial period corresponding to one wavelength ($\lambda = 0.635$ μm) is the unambiguous signature of the topological charge $\ell = 1$.

4.3. Speckle pattern

The reconstructed vectorial speckle field is reported in Fig. 5 (see Supplement 1, Fig. S2 for the reconstructed scanned object). Both components show comparable average amplitudes, with fluctuations in phase and amplitude. The spatial correlation length of the field can be roughly estimated to a couple of reconstructed pixels, i. e., in the 10–15-μm range (Fig. 5(c)), as expected for the experimental illumination conditions [28]. Beyond that distance, the SoPs are clearly uncorrelated, showing a high variety of ellipticities and orientations.

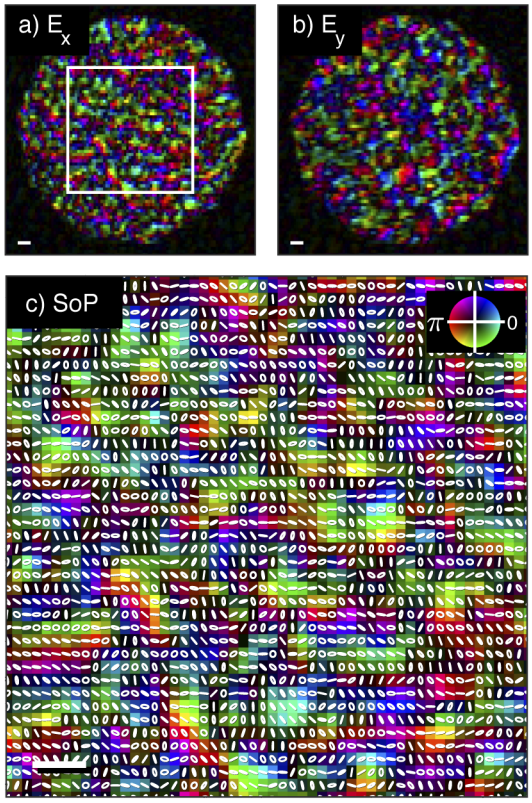

Fig. 5. Reconstructed vectorial field of the vectorial speckle. (a) E_x. (b) E_y. (c) SoP, displayed for each reconstructed pixel of the region of interest indicated in (a), superimposed in the map of E_x. Inset shows the complex value color coding, with phase encoded as hue and modulus as brightness. Scale bars are 20 μm.

Optics EXPRESS

5. Multicore fiber output

The output field of the multicore fiber is shown in Fig. 6 (see Supplement 1, Fig. S3 for the reconstructed scanned object), where the aperiodic pattern of cores of diameter of 2-μm appears clearly [27], benefiting from the spatial resolution of the technique. Within each core, the phases of the both components E_x and E_y are rather constant (Figs. 6(a) and 6(b)), giving rise to homogeneous SoPs, as shown in Fig. 6(c). The phase variation between adjacent clusters appears moderately correlated, most likely due to the rudimentary coupling. Looking at the SoP map [(Fig. 6(c)), the different cores have a quasi identical SoP, linear at 135°, confirming that the input SoP, linearly polarized at 0° experienced similar SoP rotations by all cores.

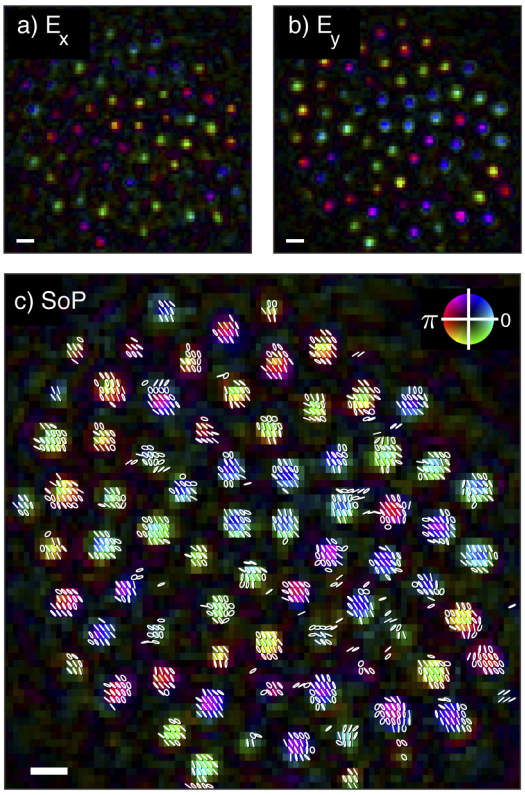

Fig. 6. Reconstructed vectorial exit field of a multicore fiber. (a) E_x. (b) E_y. (c) SoP, displayed for each reconstructed pixel of the region of interest indicated in (a), superimposed in the map of E_y. Inset shows the complex value color coding, with phase encoded as hue and modulus as brightness. Scale bars are 5 μm.

6. Discussion

For all investigated beams reported in this work, the scanned object was faithfully reconstructed (Fig. 2, Supplement 1, Figs. S1-S3), a criterion that constitutes a sign of confidence for the corresponding reconstructed vectorial field maps. Note that the isotropy of the scanned object is a necessary and critical condition for success of the method, and any anisotropy will be transferred as a bias in the reconstructed beam. However, in practice, this is not a limiting condition, since most of the resolution targets present in any microscopy labs fulfill this condition. Moreover, any spatially-structured transparent specimen that was checked to be dark between crossed polarizers irrespectively of its orientation is suitable. Note that the overall flatness, observed here for this

Optics EXPRESS

well-calibrated object, is not necessary. Given the very low level of knowledge that is required, vectorial ptychography can be considered *de facto* as a reference-free characterization method.

All beams appeared as correctly reconstructed on the basis of their respective known features, no matter their aspect, smooth (Figs. 3 and 4) vs. rough (Figs. 5 and 6) variations, continuous in intensity vs. made of discrete spots (Fig. 6). These results suggest that the method can tackle any arbitrary vectorial beam, without any *a priori* knowledge. Its spatial resolution δ is ultimately related to the numerical aperture (NA) of the objective lens according to $\delta = \lambda/(2\,\mathrm{NA})$ [23]. For a given objective lens of magnification M, the camera is usually placed at a distance d, in order to approach the condition $\mathrm{NA}/M \approx N_{\mathrm{pix}} s/(2d)$, where N_{pix} and s are the number of pixels and their size, respectively, in a given direction. In this case, assuming a two-time oversampling condition [23], the maximum lateral extend Δ of the field map that can be imaged is $\Delta \approx \lambda N_{\mathrm{pix}}/(4\,\mathrm{NA})$, so that

$$\frac{\Delta}{\delta} \approx \frac{N_{\mathrm{pix}}}{2}. \tag{5}$$

is a convenient rule of thumb. In the current work, the beams were relatively small so we used a 4×4 binning of the camera pixels in order to fit with the specificities of our instrument. Without binning we could therefore investigate 4 times larger beams. More generally in a technological context of increasing camera resolutions, the beam size does not appear to be a limitation of the present technique. This capability, together with the high spatial resolution, constitute decisive advantages for this technique.

In comparison to interferometric approaches [12–14], vectorial ptychography offers a reference-free design, ensuring experimental reproducibility and precision. Furthermore, it overcomes the main limitations of modal decomposition, thanks to its versatility. In order to illustrate this benefit, we have numerically applied a scalar modal decomposition on our reconstructed component E_y for the phase vortex (Fig. 4(b)) and for the multicore fiber (Fig. 6(b)) using a Hermite-Gauss modal basis, denoted $\mathrm{HG}_{n,m}$. Then, each field has been reconstructed by recombination of a finite number of modes. The results are summarized in Fig. 7. For the phase vortex, which is relatively smooth, 100 modes (meaning up to $\mathrm{HG}_{10,10}$) produce a rather poor reconstruction (Fig. 7(a)), with a limited spatial resolution. With 2500 modes (up to $\mathrm{HG}_{50,50}$) the reconstruction is decent (Fig. 7(b)). For the multicore fiber, 100 modes can only allow to reconstruct the central cores, in a blurry fashion, though (Fig. 7(c)). With 2500 modes, the quality of reconstruction is clearly improved, and covers all cores, with a reasonable resolution (Fig. 7(d)). These examples emphasize the unavoidable filtering effect that takes place when exploiting a limited number of modes in modal decomposition. In addition, the precision of intra and interphases measurements, assumed here perfectly know, would be undoubtedly an additional critical limitation. Thus, reaching the level of precision of vectorial ptychography would require to measure a number of modes that is redibitory in practice.

Finally, the relatively long data acquisition (typically 3 min) and computing (typically 3 hours on a laptop computer) times involved in this work work may appear limiting for some specific applications. Because all reported experiments have been performed in proof-of-principle conditions on a general-purpose microscopy setup, we believe that there is room for speed improvement, by means of an optimized design, while awaiting technological and computing progress. In this respect, the mechanically scanned object could be in principle advantageously replaced by the dynamic display of a scanned pattern, e. g., with of a micro-mirror device. Furthermore, the technique can benefit from advances in polarization-resolving cameras, now commercially available.

Optics EXPRESS

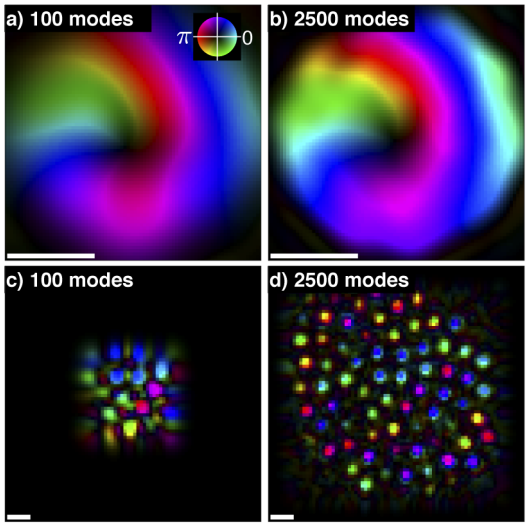

Fig. 7. Numerically reconstructed scalar fields E_y after modal decomposition on a Hermite-Gauss basis. Inset shows the complex value color coding, with phase encoded as hue and modulus as brightness. Phase vortex, for (a) 100 modes and (b) 2500 modes, to be compared with Fig. 4(b). Scale bars are 100 μm. Multicore fiber for (c) 100 modes and (d) 2500 modes, to be compared with Fig. 6(b). Scale bars are 5 μm.

7. Conclusion

We have proposed an approach aiming at measuring arbitrary vectorial light beams, based on recent progress in vectorial ptychography. The method has been experimentally demonstrated on beams of various properties, suggesting a high level of versatility. Large beams can be addressed at optical-microscopy spatial resolutions. It appears to be an ultimate diagnosis tool of light, well suited when wavefront and polarization properties are at play, in deterministic and indeterministic conditions. These results should pave the way of all novel branches of science that are based on strategies of demanding spatially-resolved measurements of light.

Funding

H2020 European Research Council (724881).

Acknowledgements

We thank Virginie Chamard (Institut Fresnel) for valuable discussions, Garaud Bouwmans (PhLAM, IRCICA, FiberTech Lille) and Herve Rigneault (Institut Fresnel) for providing us the aperiodic multicore fiber.

Disclosures

The authors declare that there are no conflicts of interest related to this article.

See Supplement 1 for supporting content.

Optics EXPRESS

References

1. C. Rosales-Guzmain, B. Ndagano, and A. Forbes, "A review of complex vector light fields and their applications," J. Opt. **20**(12), 123001 (2018).
2. A. M. Yao and M. J. Padgett, "Orbital angular momentum: origins, behavior and applications," Adv. Opt. Photonics **3**(2), 161–204 (2011).
3. G. Milione, M. P. J. Lavery, H. Huang, Y. Ren, G. Xie, T. A. Nguyen, E. Karimi, L. Marrucci, D. A. Nolan, R. R. Alfano, and A. E. Willner, "4x20 Gbit/s mode division multiplexing over free space using vector modes and a q-plate mode (de)multiplexer," Opt. Lett. **40**(9), 1980–1983 (2015).
4. Y. Kozawa and S. Sato, "Optical trapping of micrometer-sized dielectric particles by cylindrical vector beams," Opt. Express **18**(10), 10828–10833 (2010).
5. K. Toyoda, F. Takahashi, S. Takizawa, Y. Tokizane, K. Miyamoto, R. Morita, and T. Omatsu, "Transfer of Light Helicity to Nanostructures," Phys. Rev. Lett. **110**(14), 143603 (2013).
6. G. M. Lerman and U. Levy, "Effect of radial polarization and apodization on spot size under tight focusing conditions," Opt. Express **16**(7), 4567–4581 (2008).
7. R. Chen, K. Agarwal, C. J. R. Sheppard, and X. Chen, "Imaging using cylindrical vector beams in a high-numerical-aperture microscopy system," Opt. Lett. **38**(16), 3111–3114 (2013).
8. C. Maurer, A. Jesacher, S. Farhapter, S. Bernet, and M. Ritsch-Marte, "Tailoring of arbitrary optical vector beams," New J. Phys. **9**(3), 78 (2007).
9. P. Genevet, F. Capasso, F. Aieta, M. Khorasaninejad, and R. Devlin, "Recent advances in planar optics: from plasmonic to dielectric metasurfaces," Optica **4**(1), 139–152 (2017).
10. S. Rotter and S. Gigan, "Light fields in complex media: Mesoscopic scattering meets wave control," Rev. Mod. Phys. **89**(1), 015005 (2017).
11. S. Yoon, M. Kim, M. Jang, Y. Choi, W. Choi, S. Kang, and W. Choi, "Deep optical imaging within complex scattering media," Nat. Rev. Phys. **2**(3), 141–158 (2020).
12. S. Rothau, C. Kellermann, S. Mayer, K. Mantel, and N. Lindlein, "Polarization and phase-shifting interferometry for arbitrary, locally varying polarization states," Appl. Opt. **56**(5), 1422–1430 (2017).
13. M. Suzuki, K. Yamane, K. Oka, Y. Toda, and R. Morita, "Comprehensive quantitative analysis of vector beam states based on vector field reconstruction," Sci. Rep. **9**(1), 9979 (2019).
14. Z. Zhu, D. Hay, Y. Zhou, A. Fyffe, B. Kantor, G. S. Agarwal, R. W. Boyd, and Z. Shi, "Single-Shot Direct Tomography of the Complete Transverse Amplitude, Phase, and Polarization Structure of a Light Field," Phys. Rev. Appl. **12**(3), 034036 (2019).
15. Z. Yang, Z. Wang, Y. Wang, X. Feng, M. Zhao, Z. Wan, L. Zhu, J. Liu, Y. Huang, J. Xia, and M. Wegener, "Generalized Hartmann-Shack array of dielectric metalens sub-arrays for polarimetric beam profiling," Nat. Commun. **9**(1), 4607 (2018).
16. C. Schulze, A. Dudley, D. Flamm, M. Duparra, and A. Forbes, "Measurement of the orbital angular momentum density of light by modal decomposition," New J. Phys. **15**(7), 073025 (2013).
17. D. Flamm, O. A. Schmidt, C. Schulze, J. Borchardt, T. Kaiser, S. Schrater, and M. Duparra, "Measuring the spatial polarization distribution of multimode beams emerging from passive step-index large-mode-area fibers," Opt. Lett. **35**(20), 3429–3431 (2010).
18. C. Schulze, A. Dudley, D. Flamm, M. Duparra, and A. Forbes, "Reconstruction of laser beam wavefronts based on mode analysis," Appl. Opt. **52**(21), 5312–5317 (2013).
19. R. C. Jones, "A new calculus formalism for the treatment of optical systems. I. Description and discussion of the method," J. Opt. Soc. Am. **31**(7), 488–493 (1941).
20. P. Ferrand, M. Allain, and V. Chamard, "Ptychography in anisotropic media," Opt. Lett. **40**(22), 5144 (2015).
21. H. M. L. Faulkner and J. M. Rodenburg, "Movable aperture lensless transmission microscopy: A novel phase retrieval algorithm," Phys. Rev. Lett. **93**(2), 023903 (2004).
22. A. M. Maiden and J. M. Rodenburg, "An improved ptychographical phase retrieval algorithm for diffractive imaging," Ultramicroscopy **109**(10), 1256–1262 (2009).
23. J. Rodenburg and A. Maiden, "Ptychography," in *Springer Handbook of Microscopy*, P. W. Hawkes and J. C. H. Spence, eds. Springer Handbooks (Springer International Publishing, Cham, 2019), p. 2.
24. A. Baroni, M. Allain, P. Li, V. Chamard, and P. Ferrand, "Joint estimation of object and probes in vectorial ptychography," Opt. Express **27**(6), 8143–8152 (2019).
25. P. Ferrand, A. Baroni, M. Allain, and V. Chamard, "Quantitative imaging of anisotropic material properties with vectorial ptychography," Opt. Lett. **43**(4), 763–766 (2018).
26. O. Bunk, M. Dierolf, S. Kynde, I. Johnson, O. Marti, and F. Pfeiffer, "Influence of the overlap parameter on the convergence of the ptychographical iterative engine," Ultramicroscopy **108**(5), 481–487 (2008).
27. S. Sivankutty, V. Tsvirkun, O. Vanvincq, G. Bouwmans, E. R. Andresen, and H. Rigneault, "Nonlinear imaging through a Fermat's golden spiral multicore fiber," Opt. Lett. **43**(15), 3638–3641 (2018).
28. J. W. Goodman, "Statistical Properties of Laser Speckle Patterns," *Laser Speckle and Related Phenomena* J. C. Dainty, ed. , Topics in Applied Physics (Springer, Berlin Heidelberg, 1975), pp. 9–75.